Microchimica Acta (2022) 189: 46
https://doi.org/10.1007/s00604-021-05087-3

ORIGINAL PAPER

Wearable healthcare smart electrochemical biosensors based on co-assembled prussian blue—graphene film for glucose sensing

Junlin Ma[1] · Yuhang Du[1] · Yu Jiang[1] · Liuxue Shen[1] · Hongting Ma[1] · Fengjuan Lv[1] · Zewei Cui[1] · Yuzhen Pan[2] · Lei Shi[1] · Nan Zhu[1]

Received: 24 August 2021 / Accepted: 31 October 2021 / Published online: 5 January 2022

Abstract

Wearable film-based smart biosensors have been developed for real-time biomolecules detection. Particularly, interfacial co-assembly of reduced graphene oxide-prussian blue (PB-RGO) film through electrostatic interaction has been systematically studied by controllable pH values, achieving optimal PB-RGO nanofilms at oil/water (O/W) phase interface driven by minimization of interfacial free energy for wearable biosensors. As a result, as-prepared wearable biosensors of PB-RGO film could be easily woven into fabrics, exhibiting excellent glucose sensing performance in amperometric detection with a sensitivity of 27.78 μA mM^{-1} cm^{-2} and a detection limit of 7.94 μM, as well as impressive mechanical robustness of continuously undergoing thousands of bending or twist. Moreover, integrated wearable smartsensing system could realize remotely real-time detection of biomarkers in actual samples of beverages or human sweat via cellphones. Prospectively, interfacial co-assembly engineering driven by pH-induced electrostatic interaction would provide a simple and efficient approach for acquiring functional graphene composites films, and further fabricate wearable smartsensing devices in health monitoring fields.

Keywords Wearable smartsensors · Amperometric detection · O/W interfacial co-assembly · pH-induced electrostatic interaction · Prussian blue · Graphene · Real-time biomolecule monitoring

Introduction

Wearable sensing devices with skin-compatible properties have garnered great attention in glucose detection because of extremely attractive prospect in point-of-care analysis and diabetes management [1, 2]. In the meantime, functional sensing materials play a key role in achieving high-performance sensors, which has been widely exploring for integrating wearable sensing system [3–6]. Graphene (RGO) is a fascinating two-dimensional material, and diverse forms of RGO are generally studied for various applications, including sensing, catalysis, energy storage, etc. [7–14], especially of RGO nanofilm with better adaptability to complicated environments [15–18]. Oil–water (O/W) two-phase interface assembly strategy provides a simple, effective, and low-cost fabricated process for preparing RGO nanofilms that are used for blending with a controllable functional group, which would be attractive for further practical sensing application [17].

Prussian blue (PB) is generally used as 'artificial peroxidase' toward H_2O_2 sensing fields, owning to high selectivity and outstanding catalytic activity [19, 20]. In particular, PB-based wearable biosensors have been recently demonstrated to monitor body biomarkers such as glucose or alcohol, for further expressing early evaluation of healthcare status [21, 22]. Hence, it is valuable to choose PB with functionalized RGO nanofilms for achieving distinguished biosensing performance. PB modified RGO nanocomposites from traditional preparation would easily fall off during wearable or flexible process; however, one-step nanocomposite film fabrication could be essential for directly obtaining PB-RGO nanofilms in use of wearable biosensor system [23].

Herein, toluene and water were established as O/W interface to precisely guide oriented co-assembly of PB

✉ Nan Zhu
nanzhu@dlut.edu.cn

[1] Zhang Dayu School of Chemistry, State Key Laboratory of Fine Chemicals, Dalian University of Technology, Dalian, Liaoning 116024, China

[2] School of Chemical Engineering, Dalian University of Technology, Dalian 116024, Liaoning, China

nanoparticles (PBNPs) on RGO nanofilms. In terms of weak electrostatic interaction force between PBNPs and RGO nanofilms, pH variation of O/W environment was systematically discussed as facilitating co-assembly of PB-RGO films. Interestingly, PB-RGO films were mainly distributed on O/W interface, and could be easily transferred to various substrates. In order to meet wearable devices' demand, carbon cloth (CC) textile here was chosen as supporting substrate of PB-RGO films. Furthermore, wearable H_2O_2 and glucose sensors have been studied in detail, acquiring excellent biosensing performance, as well as distinguished mechanical behaviors (bending or twist testing). Additionally, wearable smart biosensing system has been designed in real-time remotely monitoring practical samples of sugary beverages or human sweat via cellphones. Therefore, this facile pH-induced O/W co-assembly engineering of wearable biosensing platform would provide a promising method for acquiring RGO-based functional films or wearable devices. Prospectively, as-designed wearable smart biosensing system would be used in remotely real-time detection for healthcare.

Experimental section

Materials and reagents

Potassium hexacyanoferrate (II) ($K_4[Fe(CN)_6]$), ferric nitrate ($Fe(NO_3)_3$), graphite powder, potassium permanganate ($KMnO_4$), potassium persulfate ($K_2S_2O_8$), phosphorus pentoxide (P_2O_5), concentrated sulfuric acid (H_2SO_4), hydrogen peroxide (H_2O_2, 30%), concentrated hydrochloric acid (HCl), acetic acid, potassium chloride (KCl), ammonia solution (30%), toluene, sodium phosphate monobasic (NaH_2PO_4) and disodium hydrogen phosphate (Na_2HPO_4) were obtained from Damao chemical reagent factory (Tianjin, China). Chitosan, dopamine (DA), uric acid (UA), ascorbic acid (AA), D-alanine, bovine serum albumin (BSA), D-(+)-glucose (≥ 99.5%), and glucose oxidase of *Aspergillus niger* (GOD) were purchased from Aladdin (Shanghai, China). Fluorine-doped tin oxide (FTO) glass, carbon cloth and dialysis bag (a cut-off of molecular weight 7000) were used as received.

Preparation of RGO

RGO was prepared according to previous report [9]. The detailed graphene oxide (GO) synthesis process could be found in Supplementary Information. Subsequently, 30 mg of dry GO was dispersed into 160 mL deionized water. Thereafter, 1.6 g of glucose was dissolved in the mixture. Then, 480 μL of ammonia solution was added into mixture reacting for 1 h at 95 °C oil bath. Afterwards, achieved black RGO suspension was filtered and washed several times until no filtrate drops. RGO was prepared ready for use.

O/W interfacial co-assembly of PB-RGO nanocomposite film

The preparation of PBNPs was detailly described in the supplementary information. PB-RGO nanocomposite film was prepared by O/W interfacial co-assembly based on adjusting pH values of water phase. Firstly, 8 mg of RGO and 30 μL of PB solution were dispersed into deionized water (20 mL) by sonication for 5 min. Adding different amounts of concentrated HCl to adjust pH. Then, 20 mL of toluene was used as oil phase. Two-phase system was transferred to an oil bath at 95 °C and stirred for 20 min. Finally, PB-RGO film was obtained at O/W interface. FTO was used to support PB-RGO film for electrochemical performance study.

Fabrication of wearable H_2O_2 sensors based on PB-RGO film

PB-RGO film synthesized at pH of 0.74 was used as active materials. CC supported PB-RGO films (CCPGF) were used as working electrode (WE). Ag/AgCl ink coated CC was used as reference electrode (RE), and fresh CC was used as counter electrode (CE). All CC electrodes were cut at 1 × 5 cm. Then, three electrodes system was integrated into commercial fabric.

Fabrication of wearable glucose sensors based on PB-RGO film

GOD solution (35 mg GOD and 10 mg BSA stabilizer were dispersed in 1 mL phosphate buffer, i.e., PBS) was mixed with chitosan solution (1 wt.% of chitosan and 2 v% of acetic acid were dissolved in PBS) in a 1:1 v/v ratio [24]. Subsequently, a 10 μL droplet of above solution was coated on WE of H_2O_2 sensors and dried under ambient conditions. Afterwards, glucose sensor was stored at 4 °C. Three electrodes were woven into diverse substrates, and Bluetooth transmission was used to collect wireless data.

Glucose detection in sugary beverages and human sweat

Cola (10.6 g sugar/100 mL) and peach flavored soda (10.1 g sugar/100 mL) were detected without treatment. The volunteer has given permission for demonstration of smart wearable textile biosensor and releasing results to public. Wearable textile glucose biosensor was woven into a textile headband. Before testing, volunteer wearing headband did in-door exercise for 15 min to generate and collect sweat. Chronoamperometric response of on-body sweat glucose

measurement was recorded at − 0.05 V (*vs.* Ag/AgCl) for 60 s at two status of pre-meal or post-meal after 1 h, respectively.

Characterization analysis

Powder X-ray diffraction (XRD) measurements were on a Rigaku D/MAX-2400 diffractometer. UV–vis measurements were carried out using a Cary Series UV–vis Spectrophotometer. TEM images were acquired using an environmental transmission electron microscope (ETEM, Titan Themis G3, Thermofisher). X-ray photoelectron spectroscopy (XPS) was measured on X-ray Photoelectron Spectrometer (ESCALAB XI + , Thermo).

Electrochemical measurements

Electrochemical measurements were carried out at room temperature by using CHI 660D electrochemical workstation under the 0.05 M phosphate buffer (PBS, pH = 7.4) containing 0.1 M KCl. PB-rGO film loaded FTO were used as WE, a Pt wire was used as CE and common glass-body Ag/AgCl (3 M KCl) as RE. Scan rate of CV was 50 mV s^{-1}, and amperometric i-t curves were carried out at − 0.05 V *vs.* glass-body Ag/AgCl (3 M KCl).

Results and discussion

Fabrication and characterization of PB-RGO film

Schematic diagram of co-assembled PB-RGO nanofilms was illustrated in Fig. 1a. RGO and PBNPs were both originally dispersed well in water phase, and PBNPs were assembled onto RGO nanofilms toward O/W interface after reaction. Additionally, O/W self-assembly of RGO or PBNPs has been prepared, separately. RGO with large energy gain could overcome effect of thermal energy, and further stably assembled on O/W interface or liquid/solid interface in forming RGO film driven by minimization of interfacial free energy (Fig. S1a and S1b) [15, 18]. On contrast, due to displacement of particles from interface induced by thermal energy, hydrophilic PBNPs with small energy gain could not assemble on O/W interface, but formed oil-in-water emulsions (Fig. S1c and S1d) [25–27].

Considering electrostatic interaction between PBNPs and RGO, O/W environmental conditions would tune PBNPs assembled on RGO films by adjusting pH value (Fig. 1b). Initially, both PBNPs (Zeta potential of − 17.2 mV) and RGO (Zeta potential of − 30.1 mV) were negatively charged in neutral environment (Fig. S2a), and electrostatic repulsion would prevent co-assembly of PB-RGO, as a result of PBNPs failing in assembled of RGO with no redox peaks in CV curve (black curve in Fig. 2a). However, electrostatic force could be easily tuned by pH of water phase (Fig. 1b). Positive charge of PBNPs will increase with acid medium adding, illustrating enhanced electrostatic interaction between PBNPs and RGO (Fig. 2b). Thus, there were more PBNPs captured on RGO nanofilms via co-assembly of O/W interface at low pH value, driven by minimization of interfacial free energy (Fig. S2b–d). Regarding various pH values in O/W system, corresponding CV curves of co-assembled PB-RGO indicated that more PBNPs exhibited better electrochemical behaviors with higher redox peak current (Fig. 2a). The optimal PB-RGO nanofilm was obtained at pH of 0.74, which was loaded onto the FTO for further study (Fig. 3a).

Subsequently, transmission electron microscopy (TEM) revealed that PBNPs were adsorbed on surface of RGO with relatively uniform distribution (Fig. 3b–d). XRD spectra of PB-RGO film displayed typical diffraction peaks of PBNPs (JCPDS no. 73–0687) and RGO (Fig. 3e, Fig. S3a–b). Main planes of (200), (220) and (400) from PBNPs, were corresponding to 2θ of 17.5, 24.8 and 35.4°, respectively [28]. Meanwhile, a broad peak centered at about 23° of (002) plane belonged to RGO, suggesting successful co-assembly induced by adjusting pH [29]. Additionally, there presented clear absorption peaks around 270 nm and 680 nm in UV–vis spectroscopy of PB-RGO, corresponding to RGO and PBNPs [9], respectively, providing sufficient evidence for co-assembled composites structure (Fig. 3f and Fig. S4).

The full XPS spectrum further revealed the presence of Fe, C, N and O elements in this PB-RGO composite (Fig. 3g). The high-resolution spectrum of C exhibited four peaks of C–C (284.8 eV), C≡N (285.7 eV), C-O (286.9 eV) and O-C = O (289.2 eV) (Fig. 3h) [30, 31]. A high-resolution spectrum of Fe possessed typical valence state located at 708.5 eV (Fe^{II} $2p_{3/2}$), 712.5 eV ($Fe^{III}2p_{3/2}$), 721 eV (Fe^{II} $2p_{1/2}$) and 724.5 eV (Fe^{III} $2p_{1/2}$), respectively, corresponding to the Fe 2p from PB in PB-RGO film (Fig. 3i) [30, 32]. Therefore, these characterizations above suggested successful co-assembly of PB-RGO film and the effectiveness of pH-mediated strategy.

Electrochemical behaviors of PB-RGO film

Electrochemical sensing properties of optimal PB-RGO film where PBNPs were captured and confined on RGO matrix have been further investigated. As shown in black curve in Fig. S5a, the apparent redox peak with formal redox potential of 0.15 V indicated good electroactivity of PB-RGO nanocomposite film [33, 34], and there exhibited well-defined reduction tendency of H_2O_2 and reach maximum current near − 0.05 V (*vs.* Ag/AgCl) in presence of 10 mM H_2O_2 (red curve in Fig. S5a). Reduction current toward

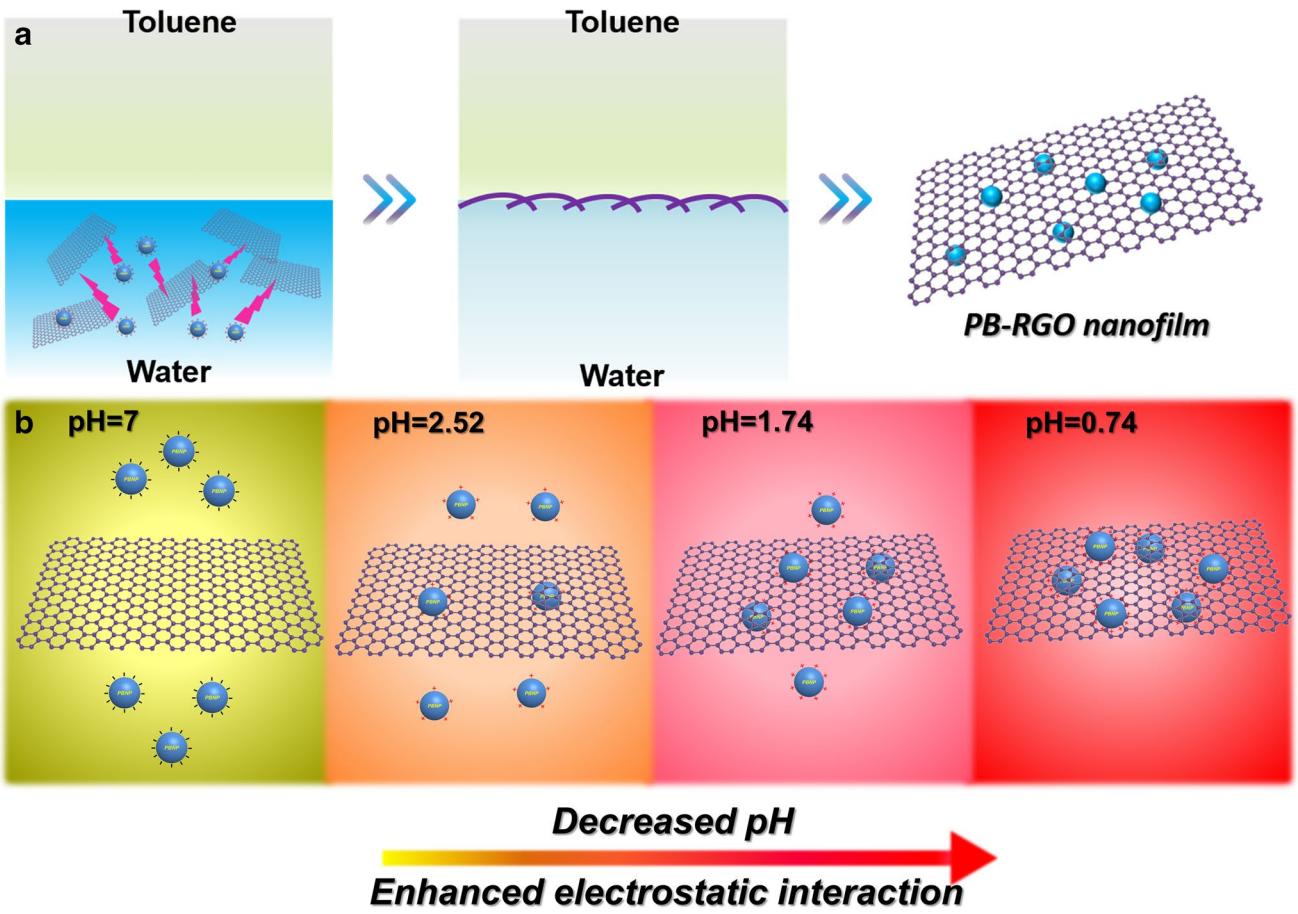

Fig. 1 Preparation of PB-RGO nanofilm. **a** Schematic diagram of co-assembled process for PB-RGO film **b** Co-assembled PB/RGO interaction under different pH value

various H_2O_2 concentration of 0–6 mM as well has been evaluated by CV and amperometric i-t curves (Fig. S5b–d). The obtained linear correlation suggested an outstanding sensitivity of 58.2 μA mM^{-1} cm^{-2} and a detection limit of 3.9 μM, reflecting excellent electrochemical sensing performance of received PB-RGO nanofilms.

Wearable H_2O_2 and glucose biosensors based on PB-RGO film

Home-made wearable woven sensing arrays integrated into fabric, has been fabricated by PB-RGO films (Fig. 4a). Figure 4b schematically depicted the profile of textile-based sensor arrays, and sensing process was based on the electrochemical reaction between PB and H_2O_2 [35]. Furthermore,

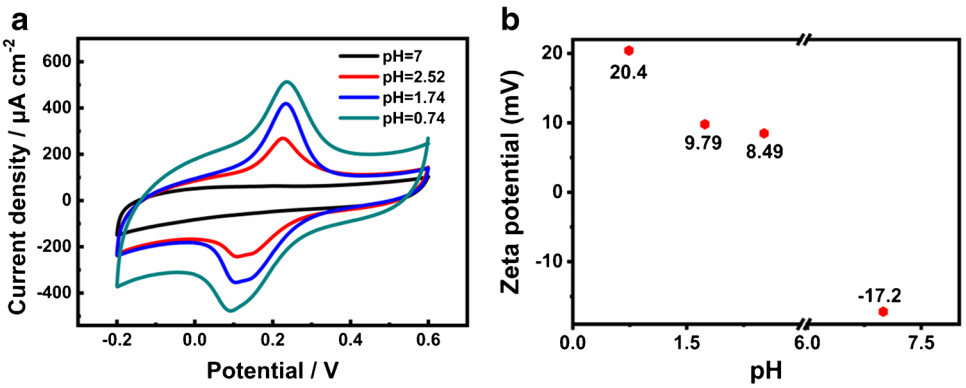

Fig. 2 Mechanism revealing of PB-RGO film. **a** CVs of PB-RGO film synthesized at different pH. **b** Zeta potential of PBNPs under different pH

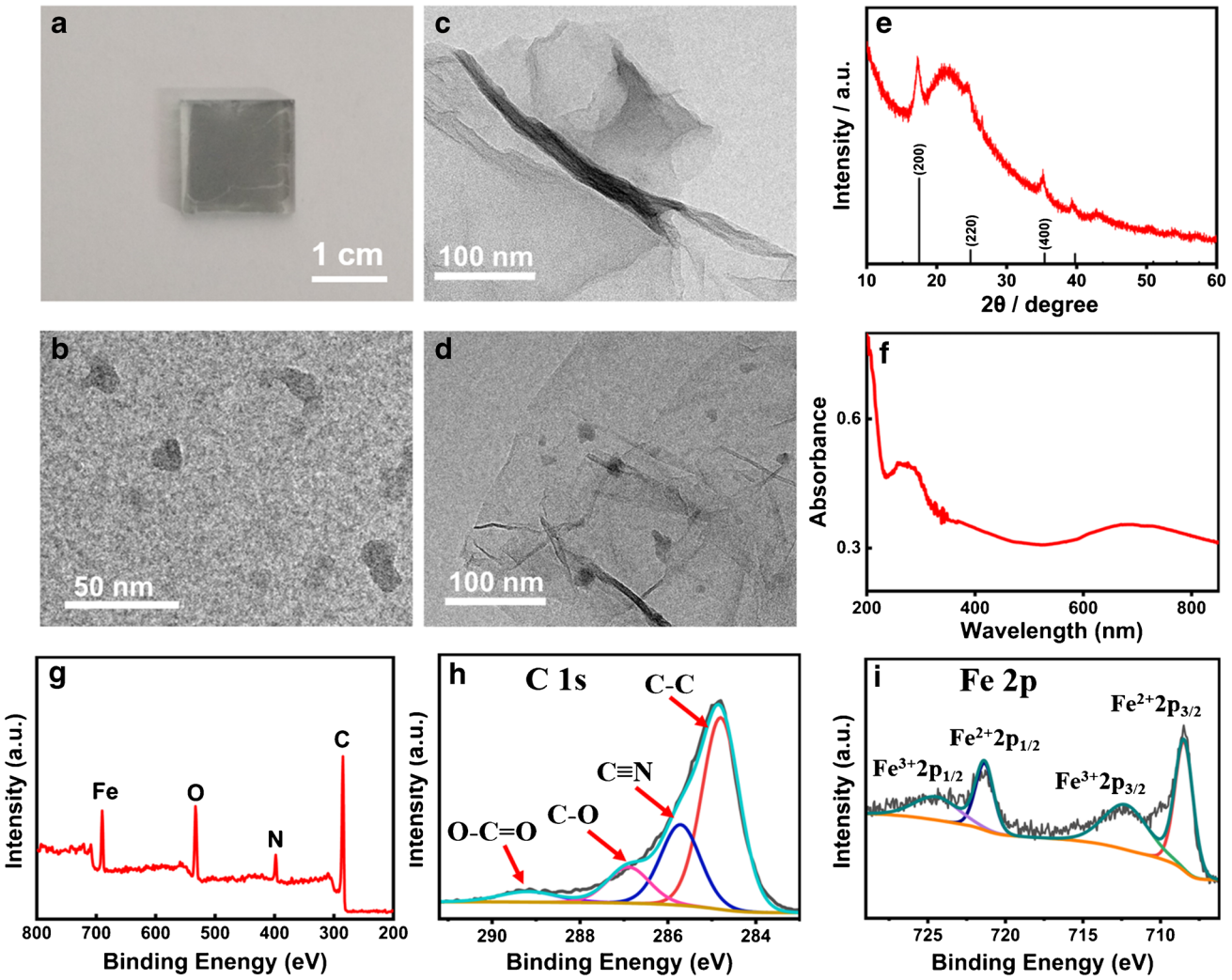

Fig. 3 Characterization of PB-RGO film. **a** Photograph of PB-RGO film loaded on FTO substrate. TEM images of **b** pure PBNPs; **c** pure RGO; and **d** PB-RGO film. **e** XRD patterns of PB-RGO film. **f** UV–vis spectra of PB-RGO film. **g** XPS survey spectra of PB-RGO composites film. **h** C 1 s XPS profile, and **i** Fe 2p XPS profile of PB-RGO composites film

there exhibited distinct H_2O_2 reduction toward different concentration from CV curves (Fig. 4c), and reduction current was gradually increasing under proportional addition of H_2O_2 probed by amperometric i-t curves (Fig. 4d). Meanwhile, electrocatalytic current linearly increased with successive addition of H_2O_2 until 6 mM, displaying an excellent correlation with a sensitivity of 60.9 μA mM^{-1} cm^{-2} and a detection limit of 1.6 μM (Fig. 4e and Fig. S6). Therefore, compared with typical flexible PB-based H_2O_2 sensors, this proposed textile sensor exhibited better comprehensive performance including higher sensitivity and wider linear range (Fig. S7) [35–37].

Figure 4f showed the response current toward 16 consecutive times of monitoring H_2O_2, and the relative standard deviation (RSD) was estimated to be 4.6%. Furthermore, RSD for 5 different sensors were less than 10%, indicating good stability of H_2O_2 sensor (Table S1). Meanwhile, anti-interferences study suggested that the H_2O_2 sensor only has a normal response to H_2O_2, effectively avoiding the interferences from other substances in the application process (Fig. S8). Besides, wearable sensor also possessed excellent mechanical performance, remaining stable signal after 90°/180° continuous bending cycles or thousands of twist cycles (Fig. 4g and 4h). These results demonstrated that fabricated PB-RGO film would be a sustainable and desired nanostructure for wearable biomolecules sensing devices.

Coupling of PB and enzymes have been proven to accomplish real-time, rapid and efficient biosensing detection, as well as superior selectivity owning to specificity of enzymes [21, 22, 24, 38]. Herein, wearable glucose sensor has been taken as example to certify advantage of PB-RGO film for biosensor application. PB-RGO film was firstly modified

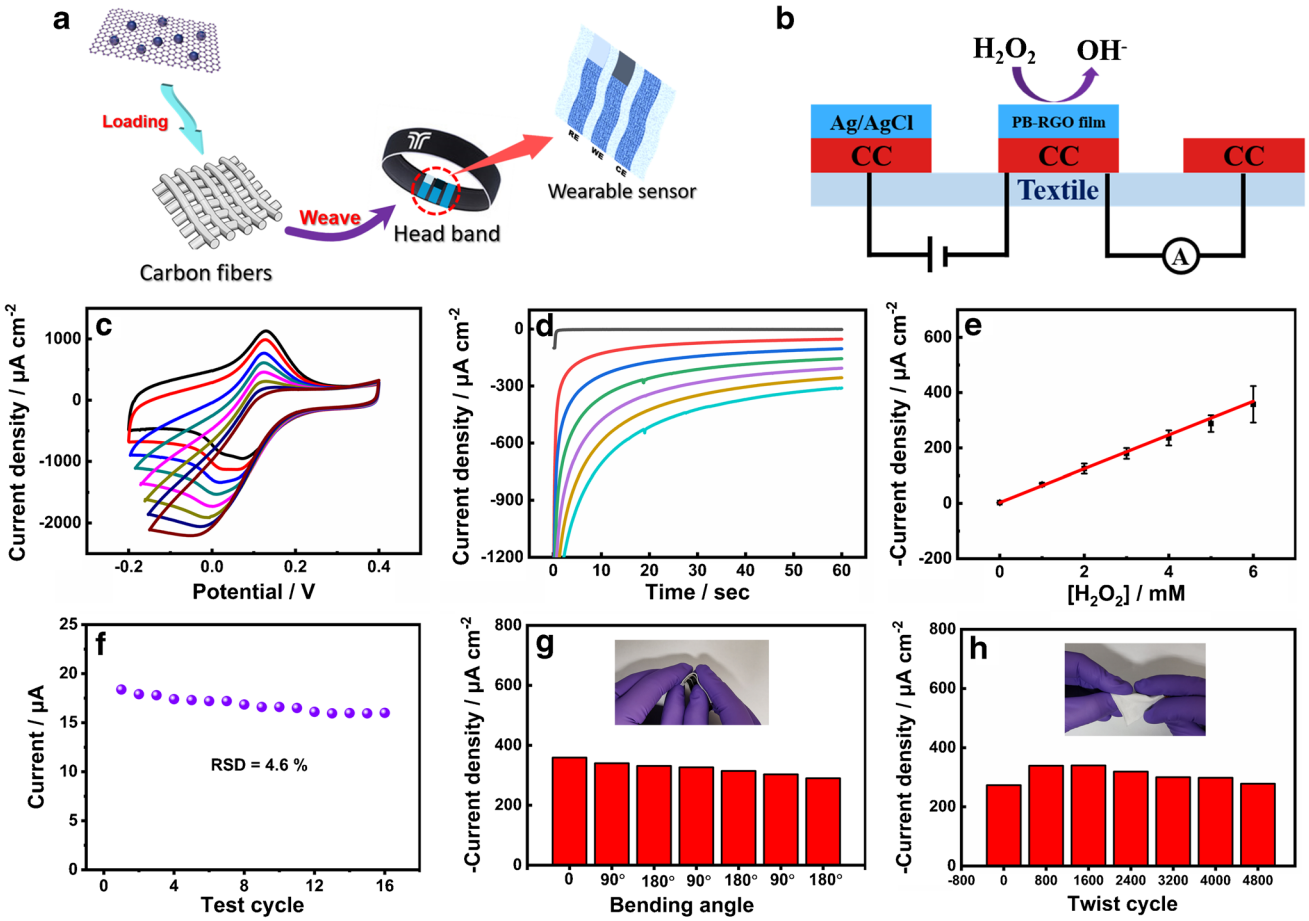

Fig. 4 Performance of wearable H_2O_2 sensors developed by PB-RGO film. **a** Schematic diagram of integrated wearable sensors. **b** Schematic diagram of sensing electrodes. **c** Electrocatalytic reduction of H_2O_2 detected by wearable sensors toward various concentration of 0–7 mM. **d** Amperometric i-t curves at − 0.05 V (*vs.* Ag/AgCl) of wearable textile H_2O_2 sensor corresponding to H_2O_2 during 0–6 mM. **e** Linear relationship of wearable H_2O_2 sensor corresponding to H_2O_2 during 0–6 mM (n = 3). **f** Reproducibility of wearable H_2O_2 sensor. **g** Bending performance of wearable H_2O_2 sensor recorded during 90°/180° continuous bending cycles. **h** Twist performance of wearable H_2O_2 sensor recorded every 800 cycles

with glucose oxidase (GOD) for manufacturing wearable glucose biosensors. The sensing mechanism was illustrated in Fig. 5a and could be described by the following biocatalytic reactions [22]:

$$\text{Glucose} + O_2 \rightarrow H_2O_2 + \text{gluconic acid.}$$

$$PB_{red} + H_2O_2 \rightarrow PB_{ox} + OH^-$$

Furthermore, a clear variation was observed in presence of 10 mM glucose compared to initial CV curve without glucose (Fig. 5b), indicating effective glucose response of wearable PB-RGO film. Moreover, response signal linearly increased toward glucose concentration until saturation from CV and i-t curves, illustrating excellent sensing performance with a sensitivity of 27.78 μA mM^{-1} cm^{-2} and a detection limit of 7.94 μM (Fig. S9 and Fig. 5c, 5d). These merits were comparable with previous reports (Table S2). Furthermore, wearable glucose sensor exhibited good stability under numerous continuous detections (RSD < 10%, Table S1), as well as superb selectivity in presence of general interfering substances including dopamine (DA), uric acid (UA), ascorbic acid (AA) and D-alanine (Fig. 5e and 5f). At the same time, there presented prolonged glucose monitoring over 2.5 h (Fig. S10). Significantly, numbers of bending or twist measurement have been carried out for wearable glucose sensors, displaying good mechanical properties (Fig. 5g and 5h). All results and discussions above demonstrated a great potential of wearable glucose sensors for actual samples detection.

Wearable healthcare smart biosensors for real-time glucose monitoring in real-life

Integrated with smartphone, wearable glucose sensing device could remotely real-time monitor actual samples, and even for healthcare application (Fig. 6a). As a result, there showed a good sensitivity and linear relationship of wearable glucose sensor remotely measured

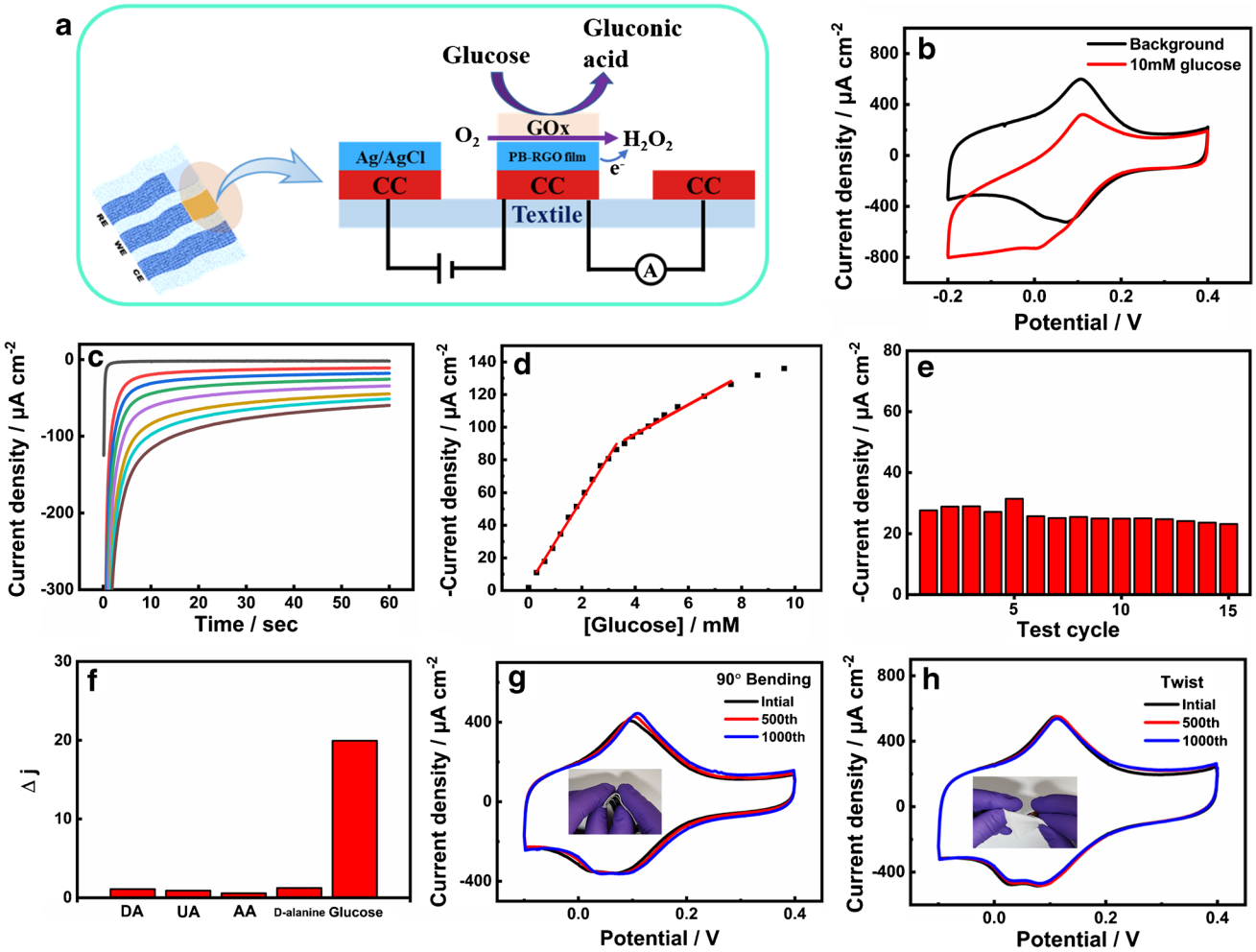

Fig. 5 Performance of wearable glucose sensors developed by PB-RGO film. **a** Schematic diagram of sensing electrodes and sensing mechanism illustration. **b** CVs of wearable textile glucose sensor in presence (red curve) and absence (black curve) of 10 mM glucose at 50 mV s^{-1}. **c** Amperometric i-t curves at − 0.05 V (*vs.* Ag/AgCl) of wearable textile glucose sensor corresponding to glucose during 0–2.1 mM in 0.3 mM increment. **d** Dependence of electrocatalytic currents of glucose on concentration under 0–10 mM glucose. **e** Stability of glucose sensor recorded at 1 mM glucose during 15 repetitive runs. **f** Selectivity of glucose sensor recorded in presence of 1 mM DA, UA, AA, D-alanine and glucose. **g** Bending performance of wearable glucose sensor recorded every 500 cycles. **h** Twist performance of wearable glucose sensor recorded every 500 cycles

by a cellphone (Fig. 6b and Fig. S11). Benefiting from facile knittability of PB-RGO film electrode, wearable sensors were further woven into various fabrics for smart monitoring of actual samples or human sweat. For example, wearable cotton glove biosensors acquired obvious feedback in remotely monitoring of cola or peach flavored soda by smartphone, reflecting high glucose concentration in beverages (Fig. 6c and 6d, Fig. S12). When wearable sensor was attached to a textile head band, it could examine slightly change of glucose level in sweat before and after meals. Thus, wearable smart biosensor exhibited increased current level in sweat as glucose concentration rising after meals, revealing reliable application for real-time healthcare in daily life (Fig. 6e and Fig. S13). Overall, these results above give impressive concept of graphene-based wearable smart biomonitoring system for future application.

Conclusion

In conclusion, O/W interfacial co-assembly of PB-RGO film through electrostatic interaction has been systematically studied by adjusting various pH values, achieving optimal PB-RGO nanofilms for wearable biosensors. As a result, as-prepared wearable textile biosensors of PB-RGO film could be easily woven into fabrics, exhibiting excellent sensing performance and impressive mechanical robustness. Furthermore, integrated smart wearable biosensing system could provide real-time, rapid,

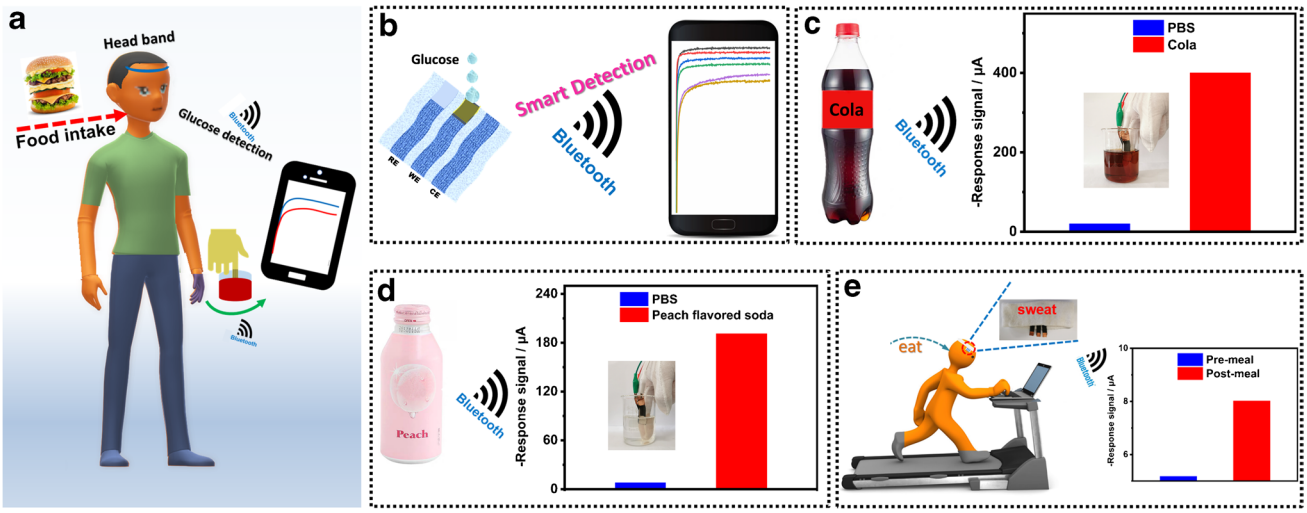

Fig. 6 Wearable smart biosensing system for real-time detection in beverages and sweat. **a** Schematic diagram of wearable smart textile glucose sensor used in practical applications. **b** Remote data acquisition measured by a smartphone. **c** Cola detection by amperometric i-t curves via a smartphone. **d** Peach flavored soda detection by amperometric i-t curves via a smartphone. **e** Sweat monitoring by chronoamperometric responses via a smartphone between pre-meal and post-meal of 1 h

efficient detection of glucose via cellphones, possessing great potential for future healthcare application. Moreover, reliable responses of glucose concentration in actual samples of beverages or human sweat have also been remotely obtained. Benefiting from the electrostatic interaction adjusted by pH value, more efforts will be devoted to assembling functional nanomaterials and diverse two-dimensional materials, and further acquiring co-assembled functional films for directly fabricating wearable sensing devices for biomolecule detection. In the future, more studies would focus on broadening film types and improving film quality for high-performance wearable sensor integration.

Supplementary Information The online version contains supplementary material available at https://doi.org/10.1007/s00604-021-05087-3.

Author contribution N.Z. conceived the idea and project. J.M. performed the experiment and data analysis. Y.D., Y.J., L.S., H.M., F.L., Z.C., Y.P., L.S. performed partial experiment and data analysis. J.M. and N.Z. jointly wrote the paper. All the authors discussed the results and commented on the manuscript.

Funding This work was supported by Dalian Science and Technology Bureau, China [Grant No. 2019J12SN54], National Natural Science Foundation of China [Grant No. 22074010], and Zhang Dayu School of Chemistry, Dalian University of Technology, China.

Declarations

Conflict of interest The authors declare no competing of interests.

References

1. Zhu BY, Li XR, Zhou L, Su B (2021) An overview of wearable and implantable electrochemical glucose sensors. Electroanalysis 33:1–10. https://doi.org/10.1002/elan.202100273
2. Kim J, Jeerapan I, Sempionatto JR, Barfidokht A, Mishra RK, Campbell AS, Hubble LJ, Wang J (2018) Wearable bioelectronics: enzyme-based body-worn electronic devices. Acc Chem Res 51:2820–2828. https://doi.org/10.1021/acs.accounts.8b00451
3. Sedighi A, Montazer M, Mazinani S (2019) Synthesis of wearable and flexible NiP0.1-SnOx/PANI/CuO/cotton towards a non-enzymatic glucose sensor. Biosens Bioelectron 135:192–199. https://doi.org/10.1016/j.bios.2019.04.010
4. Jiang Y, Xia T, Shen LX, Ma JL, Ma HT, Sun TR, Lv FJ, Zhu N (2021) Facet-dependent Cu2O electrocatalysis for wearable enzyme-free smart sensing. ACS Catal 11:2949–2955. https://doi.org/10.1021/acscatal.0c04797
5. Zheng L, Liu Y, Zhang CS (2021) A sample-to-answer, wearable cloth-based electrochemical sensor (WCECS) for point-of-care detection of glucose in sweat. Sens Actuators B Chem 343:130131. https://doi.org/10.1016/j.snb.2021.130131
6. Yao S, Swetha P, Zhu Y (2018) Nanomaterial-enabled wearable sensors for healthcare. Adv Healthcare Mater 7:1700889. https://doi.org/10.1002/adhm.201700889
7. Brugger B, Rutten S, Phan KH, Moller M, Richtering W (2009) The colloidal suprastructure of smart microgels at oil-water interfaces. Angew Chem Int Ed 48:3978–3981. https://doi.org/10.1002/anie.200900239
8. El-Kady M.F., Y. Shao, R.B. Kaner (2016) Graphene for batteries, supercapacitors and beyond. Nat. Rev. Mater. 1. https://doi.org/10.1038/natrevmats.2016.33
9. Zhu N, Han S, Gan S, Ulstrup J, Chi Q (2013) Graphene paper doped with chemically compatible prussian blue nanoparticles as nanohybrid electrocatalyst. Adv Funct Mater 23:5297–5306. https://doi.org/10.1002/adfm.201300605

10. Baringhaus J, Ruan M, Edler F, Tejeda A, Sicot M, Taleb-Ibrahimi A, Li AP, Jiang Z, Conrad EH, Berger C, Tegenkamp C, de Heer WA (2014) Exceptional ballistic transport in epitaxial graphene nanoribbons. Nature 506:349–354. https://doi.org/10.1038/nature12952
11. Jiao L, Wang X, Diankov G, Wang H, Dai H (2010) Facile synthesis of high-quality graphene nanoribbons. Nat Nanotechnol 5:321–325. https://doi.org/10.1038/nnano.2010.54
12. Shao Y, Zhang S, Wang C, Nie Z, Liu J, Wang Y, Lin Y (2010) Highly durable graphene nanoplatelets supported Pt nanocatalysts for oxygen reduction. J Power Sources 195:4600–4605. https://doi.org/10.1016/j.jpowsour.2010.02.044
13. Kavan L, Yum JH, Gratzel M (2011) Optically transparent cathode for dye-sensitized solar cells based on graphene nanoplatelets. ACS Nano 5:165–172. https://doi.org/10.1021/nn102353h
14. Wang S, Yu D, Dai L, Chang DW, Baek JB (2011) Polyelectrolyte-functionalized graphene as metal-free electrocatalysts for oxygen reduction. ACS Nano 5:6202–6209. https://doi.org/10.1021/nn200879h
15. Biswas S, Drzal LT (2009) A novel approach to create a highly ordered monolayer film of graphene nanosheets at the liquid-liquid interface. Nano Lett 9:167–172. https://doi.org/10.1021/nl802724f
16. Levendorf MP, Ruiz-Vargas CS, Garg S, Park J (2009) Transfer-free batch fabrication of single layer graphene transistors. Nano Lett 9:4479–4483. https://doi.org/10.1021/nl902790r
17. Gan S, Zhong L, Wu T, Han D, Zhang J, Ulstrup J, Chi Q, Niu L (2012) Spontaneous and fast growth of large-area graphene nanofilms facilitated by oil/water interfaces. Adv Mater 24:3958–3964. https://doi.org/10.1002/adma.201201098
18. Woltornist SJ, Oyer AJ, Carrillo JM, Dobrynin AV, Adamson DH (2013) Conductive thin films of pristine graphene by solvent interface trapping. ACS Nano 7:7062–7066. https://doi.org/10.1021/nn402371c
19. Komkova MA, Karyakina EE, Karyakin AA (2018) Catalytically synthesized prussian blue nanoparticles defeating natural enzyme peroxidase. J Am Chem Soc 140:11302–11307. https://doi.org/10.1021/jacs.8b05223
20. Karyakin AA, Karyakina EE, Gorton L (2000) Amperometric biosensor for glutamate using prussian blue-based "artificial peroxidase" as a transducer for hydrogen peroxide. Anal Chem 72:1720–1723. https://doi.org/10.1021/ac990801o
21. Zhao Y, Zhai Q, Dong D, An T, Gong S, Shi Q, Cheng W (2019) Highly stretchable and strain-insensitive fiber-based wearable electrochemical biosensor to monitor glucose in the sweat. Anal Chem 91:6569–6576. https://doi.org/10.1021/acs.analchem.9b00152
22. Kim J, Sempionatto JR, Imani S, Hartel MC, Barfidokht A, Tang G, Campbell AS, Mercier PP, Wang J (2018) Simultaneous monitoring of sweat and interstitial fluid using a single wearable biosensor platform. Adv Sci 5:1800880. https://doi.org/10.1002/advs.201800880
23. Ricci F, Palleschi G (2005) Sensor and biosensor preparation, optimisation and applications of Prussian Blue modified electrodes Biosens. Bioelectron 21:389–407. https://doi.org/10.1016/j.bios.2004.12.001
24. Bandodkar AJ, Jia W, Yardimci C, Wang X, Ramirez J, Wang J (2015) Tattoo-based noninvasive glucose monitoring: a proof-of-concept study. Anal Chem 87:394–398. https://doi.org/10.1021/ac504300n
25. Lin Y, Skaff H, Emrick T, Dinsmore AD, Russell TP (2003) Nanoparticle assembly and transport at liquid-liquid interfaces. Science 299:226–229. https://doi.org/10.1126/science.1078616
26. Hu L, Chen M, Fang X, Wu L (2012) Oil-water interfacial self-assembly: a novel strategy for nanofilm and nanodevice fabrication Chem. Soc Rev 41:1350–1362. https://doi.org/10.1039/c1cs15189d
27. Aveyard R, Binks BP, Clint JH (2003) Emulsions stabilised solely by colloidal particles Adv. Colloid Interface Sci 100–102:503–546. https://doi.org/10.1016/s0001-8686(02)00069-6
28. Wu X, Luo Y, Sun M, Qian J, Cao Y, Ai X, Yang H (2015) Low-defect Prussian blue nanocubes as high capacity and long life cathodes for aqueous Na-ion batteries. Nano Energy 13:117–123. https://doi.org/10.1016/j.nanoen.2015.02.006
29. Huang CB, Witomska S, Aliprandi A, Stoeckel MA, Bonini M, Ciesielski A, Samori P (2019) Molecule-graphene hybrid materials with tunable mechanoresponse: highly sensitive pressure sensors for health monitoring Adv. Mater 31:e1804600. https://doi.org/10.1002/adma.201804600
30. Wang J-G, Ren L, Hou Z, Shao M (2020) Flexible reduced graphene oxide/prussian blue films for hybrid supercapacitors Chem. Eng J 397:125521. https://doi.org/10.1016/j.cej.2020.125521
31. Lockett M, Sarmiento V, Balingit M, Oropeza-Guzmán MT, Vázquez-Mena O (2020) Direct chemical conversion of continuous CVD graphene/graphite films to graphene oxide without exfoliation. Carbon 158:202–209. https://doi.org/10.1016/j.carbon.2019.10.076
32. Jiang Y, Shen L, Ma J, Ma H, Su Y, Zhu N (2021) Wearable porous Au Smartsensors for on-site detection of multiple metal ions Anal. Chem 93:2603–2609. https://doi.org/10.1021/acs.analchem.0c04701
33. Kim J, Jeerapan I, Imani S, Cho TN, Bandodkar A, Cinti S, Mercier PP, Wang J (2016) Noninvasive alcohol monitoring using a wearable tattoo-based iontophoretic-biosensing system ACS Sens 1:1011–1019. https://doi.org/10.1021/acssensors.6b00356
34. Bandodkar AJ, Jeerapan I, You JM, Nunez-Flores R, Wang J (2016) Highly stretchable fully-printed CNT-based electrochemical sensors and biofuel cells: combining intrinsic and design-induced stretchability Nano Lett 16:721–727. https://doi.org/10.1021/acs.nanolett.5b04549
35. Ma J, Cui Z, Du Y, Xu Q, Deng Q, Zhu N (2021) Multifunctional Prussian blue/graphene ink for flexible biosensors and supercapacitors Electrochim. Acta 387:138496. https://doi.org/10.1016/j.electacta.2021.138496
36. Ma J, Jiang Y, Shen L, Ma H, Sun T, Lv F, Kiran A, Zhu N (2019) Wearable biomolecule smartsensors based on one-step fabricated berlin green printed arrays Biosens. Bioelectron 144:111637. https://doi.org/10.1016/j.bios.2019.111637
37. Hu JY, Lin YP, Liao YC (2012) Inkjet printed Prussian blue films for hydrogen peroxide detection. Anal Sci 28:135–140. https://doi.org/10.2116/analsci.28.135
38. Zhao J, Nyein HYY, Hou L, Lin Y, Bariya M, Ahn CH, Ji W, Fan Z, Javey A (2021) A wearable nutrition tracker. Adv Mater 33:e2006444. https://doi.org/10.1002/adma.202006444